Temporal and spatial imaging of hydrogen storage materials: watching solvent and hydrogen desorption from aluminium hydride by transmission electron microscopy†

Shane D. Beattie,*[a] Terry Humphries,[a] Louise Weaver[b] and G. Sean McGrady*[a]

Received (in Cambridge, UK) 29th April 2008, Accepted 11th June 2008
First published as an Advance Article on the web 28th July 2008
DOI: 10.1039/b807091a

An *in situ* thermal desorption study of solvated aluminum hydride (alane) by transmission electron microscopy and selected area diffraction has permitted characterisation of the structural and morphological changes during desorption of solvent and hydrogen in real-time; this powerful technique for studying hydrogen storage materials complements several others already employed.

There are extensive efforts underway worldwide to develop inexpensive and practical hydrogen storage materials for the implementation of a hydrogen-based energy economy. Perhaps the most promising candidates are light metal hydrides and their complexes.[1,2] Amongst these, the binary hydride of aluminium, alane $(AlH_3)_x$, is increasingly recognised as a leading candidate, satisfying most of the requirements laid out by the US Department of Energy.[3] Alane demonstrates impressive gravimetric and volumetric hydrogen content (around 10 wt% H and 150 kg H m^{-3}), acceptable H_2 release kinetics, and a low dehydrogenation temperature (60–150 °C).[4] Conventionally, AlH_3 is prepared by the method of Brower *et al.*,[5] involving formation of an ethereal intermediate (eqn (1)) that is converted to the polymeric hydride on annealing (eqn (2)). Alane is a kinetically stable hydride, with an equilibrium dissociation pressure of $\sim 10^5$ bar at ambient temperature, and the removal of the ether solvent (eqn (2)) converts the material from a gelatinous paste into a fine, dry powder.[5] In contrast to many metal hydride systems,[1,2] the dehydrogenation of alane is a chemically simple process, yielding aluminium metal and hydrogen gas in a single step (eqn (3)).

$$3LiAlH_4 + AlCl_3 \overset{Et_2O}{\rightarrow} 4AlH_3 \cdot nEt_2O + 3LiCl \quad (1)$$

$$4AlH_3{\cdot}nEt_2O \rightarrow 4AlH_3 + nEt_2O \quad (2)$$

$$(AlH_3)_x \rightarrow xAl + 1.5xH_2 \quad (3)$$

However, from a material standpoint, the dehydrogenation process is much more complicated, and requires characterisation by multiple techniques. The chemical and structural changes that occur in metal hydride systems during hydrogen desorption have been studied thoroughly using a range of analytical techniques including isothermal desorption,[4] differential scanning calorimetry (DSC),[6,7] thermal gravimetric analysis (TGA),[8] powder X-ray diffraction (XRD),[9,10] neutron diffraction,[11] and solid-state NMR spectroscopy (SSNMR).[12,13] All of these analytical techniques report information about the bulk properties of the sample, either at the macroscopic level, or as a statistical average at the atomic level. They are insensitive to material changes at the micron to nanometer scale. Scanning electron microscopy (SEM) has been used by several groups to study the size and morphology of metal hydride particles,[14–16] but this technique has never been used to characterise the hydrogen uptake or release characteristics of these materials *in situ*.

Transmission electron microscopy (TEM) is uniquely suited to the study of localised changes in a material at the nanometer scale. Furthermore, it is possible to study phase transitions, by *in situ* heating and imaging. As hydrogen gas is evolved, and the material undergoes a transition, structural and morphological changes can be followed as a function of temperature and time. Although metal hydrides have been previously studied using TEM,[16,17] this appears to be the first study to image–in real time—the local changes occurring during heating and desorption of H_2.

Powdered $AlH_3{\cdot}nEt_2O$ was prepared using the method developed by Brower *et al.*[5] (refer to ESI†). The powder was sprinkled onto a copper/carbon grid and transferred to a TEM heating stage. This transfer process involved brief exposure to the atmosphere. An image of the as-prepared sample is displayed in Fig. 1. The particles are coated with a thin amorphous layer of (presumably) aluminum oxide, resulting from exposure to the atmosphere during the transfer process. Residual diethyl ether is present in the sample. A selected area diffraction pattern (SADP) of the as-prepared material is shown as the inset of Fig. 1; the SADP indicates amorphous $AlH_3{\cdot}nEt_2O$, in agreement with the recent XRD study of ether-solvated alane by Graetz and Reilly.[4]

The sample was heated *in vacuo* to 80 °C inside the TEM chamber. After 90 min, small flecks were evident in some of the particles. A dark-field image (Fig. 2) revealed small crystallites emerging, appearing as bright spots embedded in the amorphous matrix. A SADP was obtained close to one of these bright-spot crystallites, and is shown as the inset to Fig. 2. The SADP reveals that the material is still largely

[a] *Department of Chemistry, University of New Brunswick, 30 Dineen Drive, Fredericton, NB, Canada E3B 6E2. E-mail: sbeattie@unb.ca; smcgrady@unb.ca*
[b] *Microscopy and Microanalysis Facility, University of New Brunswick, 10 Bailey Drive, Fredericton, NB, Canada E3B 5A3*
† Electronic supplementary information (ESI) available: Synthesis of $AlH_3{\cdot}nEt_2O$ and α-AlH_3; SADP ring measurements, powder XRD pattern of α-AlH_3. See DOI: 10.1039/b807091a

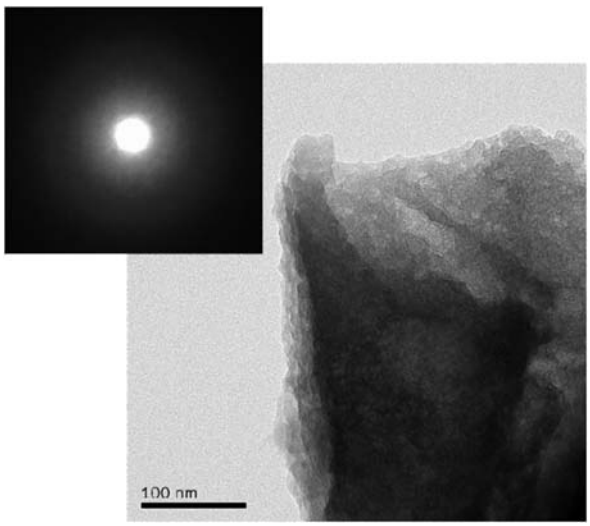

Fig. 1 TEM image and associated SADP (inset) of a freshly prepared sample of $AlH_3{\cdot}nEt_2O$.

amorphous, but nascent diffuse rings indicate a degree of crystallinity starting to evolve. The spacing of these rings corresponds to Al metal (refer to ESI† for ring measurements).[18] The number and widespread distribution of the Al crystallites indicates that the dehydrogenation of alane (eqn (3)) has occurred simultaneously in localized regions throughout the bulk material. These observations agree with the conclusions drawn by Graetz and Reilly on the basis of a DSC study;[4] namely, that the decomposition of alane is controlled by nucleation and growth of Al particles in two and three dimensions, and that the kinetics are not dependent on catalysis by surface oxide nor limited by hydrogen diffusion through an oxide barrier.

After prolonged heating for 8 h at 80 °C, the image shown in Fig. 3 was obtained. The image clearly reveals an agglomeration of Al crystallites (average size ~50 nm) in an amorphous matrix. The SADP displayed as an inset to Fig. 3 indicates a high degree of crystallinity, with the ring spacing corresponding

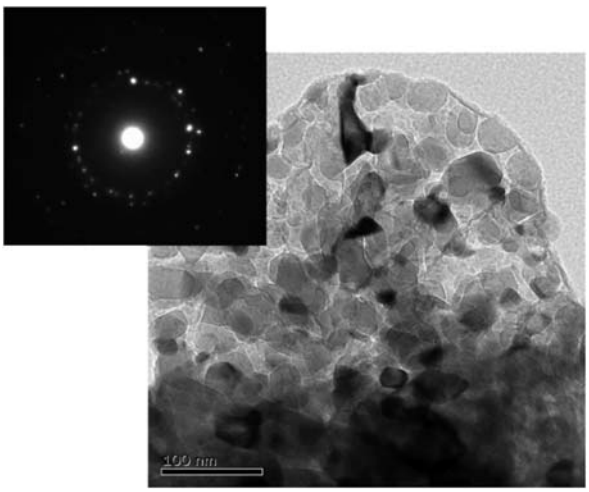

Fig. 3 TEM image and SADP (inset) of a fully decomposed sample of $AlH_3{\cdot}nEt_2O$.

to Al metal[18] (refer to ESI† for ring measurements), confirming the decomposition reaction (eqn (3)) to be complete. The more diffuse features towards the centre of this SADP indicate the presence of a residual amorphous phase; as-yet unidentified.

Previous studies by Graetz and Reilly[4,6] indicate that $AlH_3{\cdot}nEt_2O$ loses ether to produce α-AlH_3 before decomposing to Al. We were unable to identify definitively this solvent-free α-AlH_3 phase during the experiments described above. However, a faint SADP was obtained, with features that may correspond to the α-AlH_3 (Fig. S1 in ESI†). In order to clarify the origin of these features, a follow-up series of TEM experiments was conducted, this time using ether-free α-AlH_3 (refer to ESI† for details), whose identity was confirmed *ex situ* by powder XRD[19] (Fig. S2 in ESI†). Although the α-AlH_3 sample showed well defined peaks in the *ex situ* powdered XRD pattern, it was difficult to find a SADP corresponding to α-AlH_3 with the TEM. After several inconclusive attempts, it was realised that α-AlH_3 is sensitive to the high energy TEM electron beam. This is perhaps unsurprising, as previous

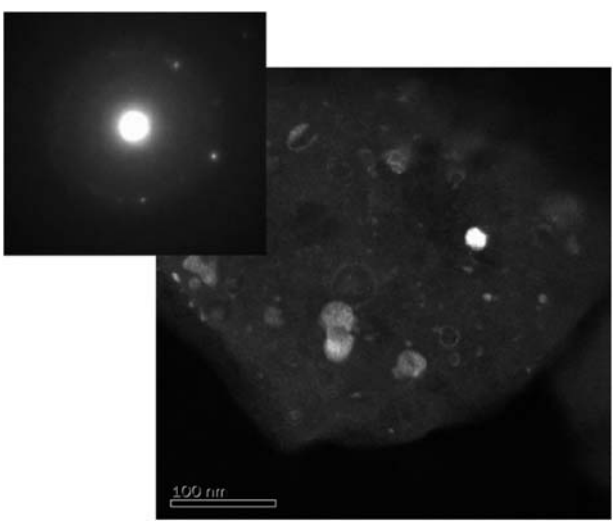

Fig. 2 Dark-field image and associated SADP (inset) after heating $AlH_3{\cdot}nEt_2O$ for 90 min at 80 °C.

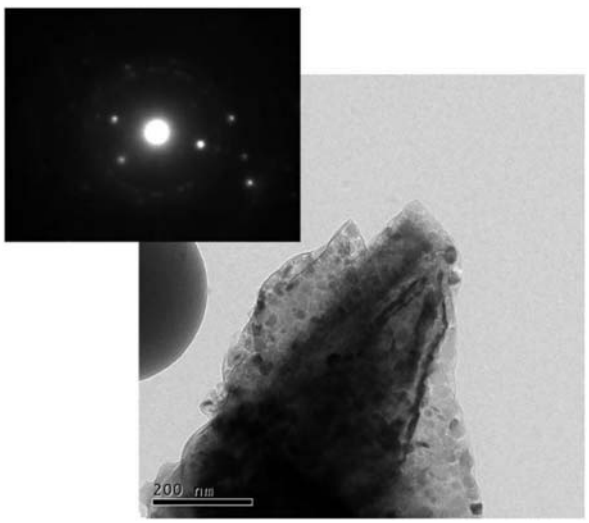

Fig. 4 TEM image and SADP (inset) of α-AlH_3 after short exposure to the TEM beam.

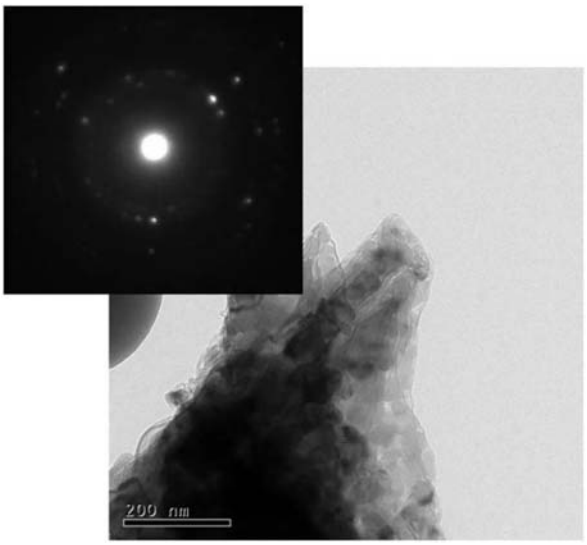

Fig. 5 TEM image and SADP (inset) of the same area as Fig. 4 after prolonged exposure to the TEM beam.

studies have shown the decomposition of α-AlH_3 to Al to be accelerated by exposure to UV light,[14] and to 1 MeV ^{60}Co γ-irradiation.[20] Although the sample decomposes within seconds on exposure to the electron beam, ultimately, a SADP that clearly corresponds to α-AlH_3 was obtained (Fig. 4).

The SADP in Fig. 4 contains contributions from both α-AlH_3 and metallic Al (refer to ESI† for ring measurements). It is difficult to identify unambiguously certain features, as both materials have similar *d*-spacings. However, α-AlH_3 has a unique reflection at 3.28 Å, which is clearly observed in the SADP of Fig. 4. The 3.28 Å reflection was observed previously (refer to ESI,† Fig. S1) during the initial stages of $AlH_3{\cdot}n Et_2O$ decomposition, however, the SADP was diffuse and it was difficult to definitively identify the α-AlH_3 phase.

Fig. 5 shows the same area as Fig. 4 and corresponding SADP following further exposure to the electron beam. Of particular note in Fig. 5 are the larger grains, the absence of the earlier spots at 3.28 Å, and the strong Al doublet rings at 2.338 and 2.024 Å (refer to ESI† for ring measurements). These features unambiguously point to the disappearance of α-AlH_3 and the emergence of metallic Al in its place.

To the best of our knowledge, this is the first real-time, *in situ* study by TEM of hydrogen desorption from a metal hydride.‡ The high resolution of the technique, in combination with the ability to obtain localised diffraction patterns, has allowed an *in situ* temperature and time resolved study of the structural and morphological changes that occur during desolvation and hydrogen desorption. Decomposition of α-AlH_3 occurs spontaneously at localized sites throughout the bulk material, and is not initiated by nucleation at the surface of the particles. Furthermore, the rate of decomposition is not controlled by diffusion of H_2 to the surface. Amorphous $AlH_3{\cdot}n Et_2O$ loses the solvent to produce α-AlH_3, which then proceeds rapidly to lose H_2, leaving behind crystalline Al with a particle size of *ca.* 50 nm. In spite of the sensitivity of the material to the electron beam valuable information has been obtained about each of the decomposition steps involved in the dehydrogenation and the structural evolution of α-AlH_3 – at the nanoscopic level – in real-time. Although we have been successful in studying AlH_3 by this technique, the sensitivity of the sample to the high energy TEM electron beam may prove to be a more serious problem with other metal hydrides.

We thank NSERC, CFI, NBIF and HSM Systems for financial support of this research.

Notes and references

‡ A time-resolved movie of the decomposition of α-AlH_3 to Al is available on the McGrady group website: http://www.unb.ca/fredericton/science/chem/smcgrady/news/index.html

1 W. Grochala and P. P. Edwards, *Chem. Rev.*, 2004, **104**, 1283.
2 S. Orimo, Y. Nakamori, J. R. Eliseo, A. Züttel and C. M. Jensen, *Chem. Rev.*, 2007, **107**, 4111.
3 S. Satyapal, J. Petrovic, C. Read, G. Thomas and G. Ordaz, *Catal. Today*, 2007, **120**, 246.
4 J. Graetz and J. J. Reilly, *J. Phys. Chem. B*, 2005, **109**, 22181.
5 F. M. Brower, N. E. Matzek, P. F. Reigler, H. W. Rinn, C. B. Roberts, D. L. Schmidt, J. A. Snover and K. Terada, *J. Am. Chem. Soc.*, 1976, **98**, 2450.
6 J. Graetz and J. J. Reilly, *J. Alloys Compd.*, 2006, **424**, 262.
7 M. Resana, M. D. Hamptona, J. K. Lomnessa and D. K. Slattery, *Int. J. Hydrogen Energy*, 2005, **30**, 1417.
8 J. Wang, A. D. Ebner, T. Prozorov, R. Zidan and J. A. Ritter, *J. Alloys Compd.*, 2005, **395**, 252.
9 B. Bogdanovic, R. A. Brand, A. Marjanovic, M. Schwickardi and J. Tölle, *J. Alloys Compd.*, 2003, **350**, 246–255.
10 E. H. Majzoub and K. J. Gross, *J. Alloys Compd.*, 2003, **356–357**, 363.
11 S. Singh, S. W. H. Eijt, J. Huot, W. A. Kockelmann, M. Wagemaker and F. M. Mulder, *Acta Mater.*, 2007, **55**, 5549.
12 V. P. Tarasov, Yu. B. Muravlev, S. I. Bakum and A. V. Novikov, *Dokl. Phys. Chem.*, 2003, **393**, 353.
13 O. J. Zogait, M. Punkkinen, E. E Ylinent and B. Stalinski, *J. Phys.: Condens. Matter*, 1990, **2**, 1941.
14 P. J. Hereley, S. O. Christofferson and J. A. Todd, *J. Solid State Chem.*, 1980, **35**, 391.
15 B. Bogdanovic, R. A. Brand, A. Marjanovic, M. Schwickardi and J. Tölle, *J. Alloys Compd.*, 2000, **302**, 36–58.
16 A. Leon, O. Kircher, H. Rosner, B. Decamps, E. Leroy, M. Fichtner and A. P. Guegan, *J. Alloys Compd.*, 2006, **414**, 190.
17 M. Felderhoff, K. Klementiev, W. Grunert, B. Spliethoff, B. Tesche, J. M. Bellosta von Colbe, B. Bogdanović, M. Hartel, A. Pommerin, F. Schüth and C. Weidenthalera, *Phys. Chem. Chem. Phys.*, 2004, **6**, 4369.
18 JCPDS-ICCD PDF-2 Database #4-787, 1996.
19 JCPDS-ICCD PDF-2 Database #14-1436, 1996.
20 P. J. Herley and R. H. Irwin, *J. Phys. Chem. Solids*, 1978, **39**, 1013.

